Resonant, Plasmonic Raman Enhancement of α-6T Molecules Encapsulated in Carbon Nanotubes

Author(s):
Wasserroth, Soeren; Heeg, Sebastian; Müller, Niclas S.; Kusch, Patryk; Hübner, Uwe; Gaufrès, Etienne; Tang, Nathalie Y.-W.; Martel, Richard; Vijayaraghavan, Aravind; Reich, Stephanie

Publication date:
2019

Permanent link:
https://doi.org/10.3929/ethz-b-000342533

Originally published in:
The Journal of Physical Chemistry C 123(16), https://doi.org/10.1021/acs.jpcc.9b01600

THE JOURNAL OF PHYSICAL CHEMISTRY C

Article

Cite This: J. Phys. Chem. C 2019, 123, 10578−10585

pubs.acs.org/JPCC

Resonant, Plasmonic Raman Enhancement of α-6T Molecules Encapsulated in Carbon Nanotubes

Sören Wasserroth,[†] Sebastian Heeg,[‡,⊥] Niclas S. Mueller,[†] Patryk Kusch,[‡] Uwe Hübner,[§] Etienne Gaufrès,[∥] Nathalie Y.-W. Tang,[∥] Richard Martel,[∥] Aravind Vijayaraghavan,[‡] and Stephanie Reich*[,†]

[†]Institut für Experimentalphysik, Freie Universität Berlin, Berlin 14195, Germany

[‡]School of Materials, The University of Manchester, Manchester M13 9PL, U.K.

[§]Leibniz Institute of Photonics Technology, Jena 07745, Germany

[∥]Regroupement Québécois sur les matériaux de pointe and Département de Chimie, Université de Montréal, Montréal, Québec H3C 3J7, Canada

[⊥]Photonics Laboratory, ETH Zürich, Zürich 8093, Switzerland

ABSTRACT: Surface-enhanced Raman scattering (SERS) and resonant Raman scattering are widely used techniques to enhance the Raman intensity of molecules and nanomaterials by several orders of magnitude. In SERS, typically, molecules are investigated and their intrinsic resonance is often ignored while discussing the plasmonic enhancement. Here, we study α-sexithiophenes encapsulated in carbon nanotubes placed in the center of a nanodimer. By dielectrophoretic deposition, we place the nanotubes precisely in the center of a plasmonic gold nanodimer and observe SERS enhancement from individual tube bundles. The encapsulated molecules are not subjected to chemical enhancement because of the protective character of the nanotube. Polarization-dependent Raman measurements confirm the alignment of the molecules within the carbon nanotubes (CNTs) and reveal the influence of the plasmonic near field on the molecule's Raman intensity. We investigate the encapsulated molecules in small CNT bundles with and without plasmonic enhancement and determine the molecular and plasmonic resonance by tuning the excitation wavelength. We observe a strong red shift of the maximum Raman intensity under plasmonic enhancement toward the plasmon resonance.

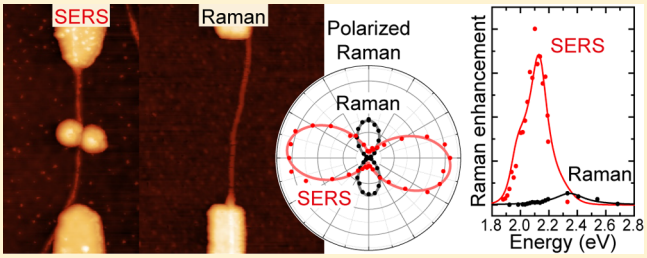

1. INTRODUCTION

Raman scattering is a powerful chemically sensitive technique to analyze materials and detect the presence of target molecules. Unfortunately, the Raman scattering cross section of materials is very weak ($\sigma_R \approx 10^{-31}$ cm^2/ster·mol), typically requiring large amounts of analytes for detection.[1] To overcome this disadvantage, surface-enhanced Raman scattering (SERS) and resonant Raman scattering are widely used to enhance the analytes' Raman intensity.[2−5] In SERS, metallic nanoparticles generate plasmonic near fields that act as external resonances for the analyte. Large enhancement factors were reported, giving, under favorable conditions, single-molecule sensitivity.[6−9] Single-molecule experiments combine SERS enhancement (~10^{10} enhancement factor) with Raman resonances (10^4 enhancement factor) to achieve the required sensitivity.[2,10]

Typical SERS substrates are rough metal surfaces or ensembles of metallic nanoparticles.[5,11−14] The incident laser excites localized surface plasmons producing plasmonic near fields around the nanoparticles.[2] The near fields enhance the incoming and scattered light of the Raman process. An additional increase in the analyte's Raman intensity is often attributed to the environment of the investigated material and is called chemical enhancement.[2] It describes the chemical interaction between the metal and the investigated material. The analytes studied by SERS are usually molecules that are dispersed on surfaces or anchored on the metal surface. Therefore, the position and orientation of the molecules remain unknown or arbitrary. To achieve highest enhancement in SERS, however, it is pivotal to align the molecular orientation with the polarization of the plasmonic near field.[15,16]

Resonant Raman scattering exploits the electronic excitations of the investigated material. By choosing a laser wavelength that matches an electronic or optical transition energy of the material, the Raman intensity gets enhanced.[3] Resonant Raman scattering is sensitive to single groups of the analyte (e.g., in proteins). The intrinsic resonances are sensitive to the dielectric environment and to subtle changes of the molecular configuration.[5,17] When using literature values

Received: February 19, 2019
Revised: April 1, 2019
Published: April 2, 2019

DOI: 10.1021/acs.jpcc.9b01600
J. Phys. Chem. C 2019, 123, 10578−10585

for the intrinsic resonance of a molecule, the surrounding medium needs to be considered. As the resonances of molecules and low-dimensional nanostructures are particularly susceptible to shifts due to dielectric screening, two systems may only be compared if they are subject to the same chemical environment.[18]

Analytes in SERS experiments possess intrinsic Raman resonances in addition to the external plasmonic enhancement. In the discussion of SERS, however, intrinsic resonances and their variation with the molecule's dielectric surrounding are often neglected, and enhancement factors are determined by referring the SERS intensity to Raman scattering on molecules in a solution or powder form. For a proper assignment of the enhancement factor, it is important to consider both intrinsic and extrinsic enhancement in SERS measurements because each affects the total intensity and the energetic position of the plasmonic and molecular resonance.

With wavelength-dependent Raman measurements, it is possible to simultaneously study the molecular and plasmonic resonances and ultimately disentangle their individual contributions to the Raman enhancement. For the nonresonant Raman reporter graphene suspended over a gold dimer, the plasmonic resonance was measured for a single hotspot.[19,20] To investigate the interplay of intrinsic and plasmonic resonance, it was shown that carbon nanotubes (CNTs) can reliably be placed in plasmonic hot spots by dielectrophoretic deposition.[15,21−23] Using functionalized CNTs allows molecules to be brought in the plasmonic hotspot. Different endohedral and exohedral functionalization approaches are used to attach molecules to CNTs.[24] Encapsulating molecules inside of the CNT has the advantage that the molecules are chemically protected from the environment. The CNT wall also protects the molecules against reactive oxidizing species that prevent photobleaching and enable long optical measurement on the same system. Another advantage is the alignment of some molecules, for example, rodlike molecules such as α-sexithiophene (α-6T), inside of the CNT. In this way, the orientation of the molecules may be determined from microscopy images.[25] Some of us showed in SERS experiments at fixed wavelengths that encapsulated α-6T do not experience chemical enhancement when placed inside a gold dimer, making them ideal model systems for studying the combination of plasmonic and intrinsic resonances.[26]

Here, we present an extensive Raman study of α-6T encapsulated in CNTs (α-6T@CNT). We chose these molecules because of their high Raman cross section and the alignment inside the CNTs.[27,28] Using the nanotubes as carriers, the encapsulated molecules were deposited on a substrate with gold nanodimers by dielectrophoretic deposition. With this technique, we were able to precisely place small bundles of nanotubes into the dimer gap. We refer to the plasmonic enhanced molecules as α-6T@CNT-Au. We performed resonant Raman measurements on the encapsulated molecules with and without plasmonic enhancement by a gold nanodimer. We measured the molecular resonance of the encapsulated molecules at 528 nm without plasmonic enhancement. The plasmonically enhanced α-6T@CNT-Au showed maximum enhancement at 590 nm. Polarization-dependent Raman measurements showed that the molecules are aligned with the CNT axis. For the α-6T@CNT-Au inside of the plasmonic dimer gap, the maximum intensity occurred for polarization along the dimer axis and therefore the plasmonic near-field polarization. From the resonant Raman measurements and the number of molecules subject to plasmonic enhancement, we were able to determine the enhancement factor of our system to be on the order of 10^5. In the presence of plasmonic enhancement, the largest Raman intensity was red-shifted by $\Delta E = 0.22$ eV from the molecular resonance.

2. EXPERIMENTAL SECTION

2.1. α-6T Encapsulation. Plasma-torch single-walled CNTs (Raymor RN-020) with a mean diameter of 1.3 nm (diameters between 0.9 and 1.5 nm) were filled with α-6T molecules. The single-walled CNTs were purified and cut in piranha solution. The sexithiophene molecules were diluted in toluene and the CNTs were added to them. The solution was refluxed at elevated temperatures overnight. Afterward, the solution was dispersed and filtered several times to remove free molecules. The filling process is described in more detail in ref 27. α-6T molecules are rodlike and form a head-to-tail row inside of the nanotube aligned along the CNT axis, as was confirmed by transmission electron microscopy.[25,28] If the diameter of the CNT is larger than 1.1 nm, two rows of molecules form inside of the CNT side by side. The interaction between the CNT and the encapsulated molecules is mediated by van der Waals forces.

2.2. Fabrication of the Plasmonic Nanostructures. The plasmonic nanostructures were fabricated by e-beam lithography with a shaped beam writer SB350 OS (50 keV, Vistec Electron Beam GmbH) on top of a 290 nm SiO_2/Si substrate. Metallization was carried out by thermal evaporation of 5 nm Ti and 75 nm Au, followed by lift-off. Figure 1a shows a sketch of the investigated system. Two gold discs with a diameter of 100 nm and a height of 80 nm form dimers. The investigated dimers have interparticle gaps of 20 nm. The dimers were fabricated in the center of two gold electrodes that are used for the dielectrophoretic deposition of the filled CNTs. The electrodes are separated by approximately 850 nm. The dimers are oriented with an angle of 70° with respect to the electrodes. This orientation yields higher near-field enhancement of the Raman modes compared to an angle of 90° because the near field couples more strongly to the α-6T@CNT-Au.[15,22] We investigated filled CNTs without plasmonic structures for reference purposes using electrodes separated by 1.3 μm.

2.3. Dielectrophoretic Assembly of α-6T@CNT into Plasmonic Hotspots. The filled CNTs were brought into solution and subsequently drop-casted on the lithographic structures. An alternating electric field was applied on the electrodes inducing a force on the CNTs aligning and depositing them between the electrodes.[21] Depending on the concentration and bundling of the CNTs, we deposited small bundles of CNTs into the plasmonic hotspots at the dimer gap. We used a Park Systems XE-150 AFM to measure the topography and height profiles of the α-6T@CNT and chose areas where only a single bundle of filled CNTs is connecting the electrodes passing through the center of the gold dimer (Figure 1b,d). For the reference CNTs without plasmonic nanostructures, we chose a bundle with a similar height to compare both measurements (Figure 1c,e).

2.4. Wavelength- and Polarization-Dependent Raman Measurements. The wavelength-dependent Raman measurements were performed with a tunable dye laser with different dyes covering the wavelength range of 560−670 nm. Additional measurements were performed using an ND:YAG

DOI: 10.1021/acs.jpcc.9b01600
J. Phys. Chem. C 2019, 123, 10578−10585

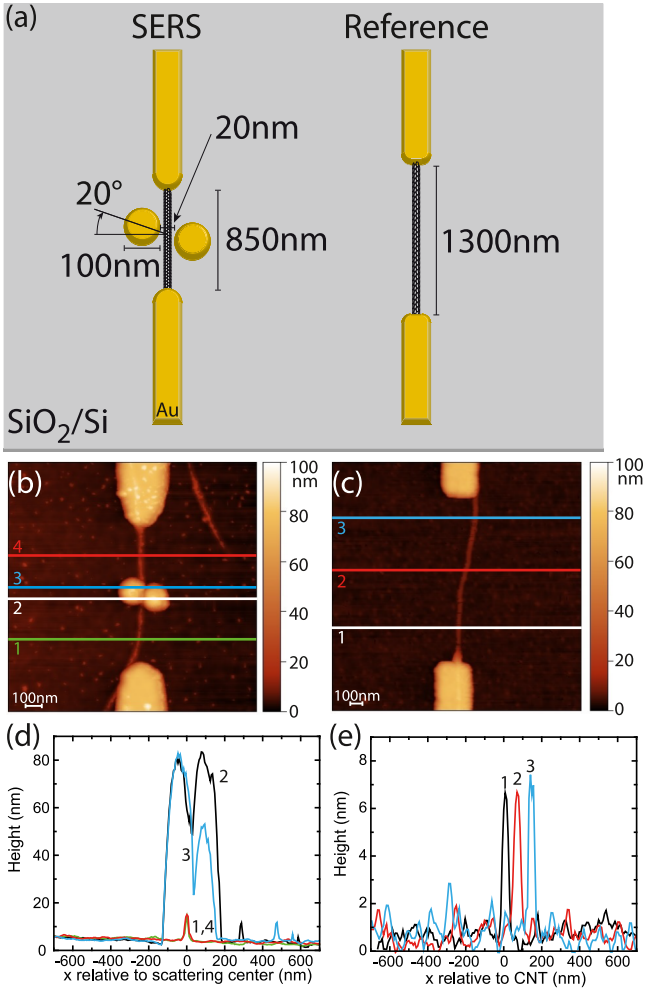

Figure 1. (a) Sketch of the α-6T@CNT-plasmonic system (left) together with the bare α-6T@CNT reference (right) for comparison. The gold electrodes were used for the dielectrophoretic deposition of the filled nanotubes. The left part shows the CNT bundle going through the center of the plasmonic dimer, whereas the right part shows the reference bundle without the plasmonic system. Atomic force microscope (AFM) topography image of (b) plasmonic system and (c) reference. Horizontal lines indicate the position of the respective height profiles shown in (d,e).

laser at 532 nm and single lines of an Ar/Kr laser extending the excitation range down to 461 nm. The power in the laser focus (<1 μm^2) was kept at 20 μW on the CNTs interfaced with the plasmonic dimer and 100 μW on the reference α-6T@CNT to avoid damaging the α-6T@CNT. A λ/2-waveplate and an analyzer were used to perform the polarization-dependent measurements (see ref 19). When comparing different peak intensities as a function of excitation energy and polarization, we always refer to integrated peak areas obtained from one (6T) or several (CNT) Lorentzian fits. The spectra were acquired with a Jobin Yvon T64000 HORIBA spectrometer with a silicon charge coupled detector. The light was focused on the sample with a 100× objective (NA = 0.9) in backscattering configuration. To ensure that the α-6T@CNT remained in focus at all times, we maximized the Raman signal by varying the distance between the objective and the sample in steps of 100 nm using a piezo stage (PI E-710). To account for changes in the response of the detector and other optical components, we measured the Raman spectrum of diamond for calibration. The integrated intensity of the α-6T@CNT Raman mode was normalized by the integrated intensity of diamond at the same wavelength and spectrometer configuration.

2.5. Simulation. We simulated the extinction cross section of a gold dimer with the dimensions given above including the substrate. The gold particles were assumed to have the shape of half ellipsoids. The simulations were carried out with the commercial finite-difference time-domain (FDTD) package Lumerical FDTD Solutions. The cross section was obtained with a combination of power monitors and a total-field scattered-field source. For more details on the simulation methodology, we refer to ref 26.

3. RESULTS AND DISCUSSION

We performed wavelength- and polarization-dependent Raman measurements on small bundles of α-6T@CNT-Au to investigate the influence of the plasmonic near field on the intrinsic resonance of the encapsulated molecules. Figure 2a presents the Raman spectra of the reference α-6T@CNT bundle at different wavelengths with polarization along the nanotube axis. An excitation wavelength of 532 nm (green) provides spectra with strong molecular and CNT Raman modes. The molecular mode of α-6T on which we will focus in this work is located at $\omega_{\alpha\text{-}6T} \approx 1450\ cm^{-1}$.[27] The CNT Raman modes, namely, the G, D, and radial breathing mode (RBM), are also strong at this wavelength, while they are much weaker at an excitation wavelength of 638 nm, indicating enhancement by optical resonance. The silicon modes from the substrate are visible as well.

For the α-6T@CNT-Au bundle placed inside the dimer cavity (Figure 2b), a similar behavior is observed when the polarization is aligned with the nanotube compared to the reference α-6T@CNT. Upon rotating the polarization to the dimer axis, the α-6T and CNT Raman modes almost vanish at an excitation wavelength of 532 nm. In contrast, the α-6T and CNT Raman modes are strongly enhanced at λ = 638 nm excitation due to the plasmonic hotspot that is activated in this energy range.[20,29] The D mode of the CNTs is much stronger in the plasmonically enhanced spectrum. Plasmon-activated D modes due to the strong electric field localization by the plasmon in the dimer gap were observed previously.[19,23,30]

For both the plasmonically enhanced and the reference α-6T@CNT bundles, we observe a prominent RBM in the investigated wavelength range. For the reference CNTs, the RBM is at $\omega_{ref}^{RBM} = 190\ cm^{-1}$ and the plasmonically enhanced CNT frequency of ω_{SERS}^{RBM} is 183 cm^{-1}. Previous experiments on α-6T@CNT showed that the filling of the nanotubes leads to a small shift of the RBM frequency compared to unfilled tubes, which is why we avoid to specify the corresponding CNT species here.[27] The chirality of the nanotube does not influence the Raman intensity of the encapsulated molecules.[27]

A phenomenon often observed in SERS is blinking or SERS intensity fluctuations. Blinking of Raman modes, for example, was observed in the graphene D-modes indicating local changes in the gold surface.[19] To rule out blinking, we record the plasmonically enhanced Raman intensity as a function of time for the α-6T@CNT-Au system. We chose an excitation wavelength of λ = 585 nm where we observe strong plasmonic enhancement (see section 3.3). During a total measurement time of 300 s, we recorded a Raman spectrum every 5 s and observed constant Raman intensities, as shown in Figure 3. The absence of fluctuations in the Raman intensities confirms

DOI: 10.1021/acs.jpcc.9b01600
J. Phys. Chem. C 2019, 123, 10578−10585

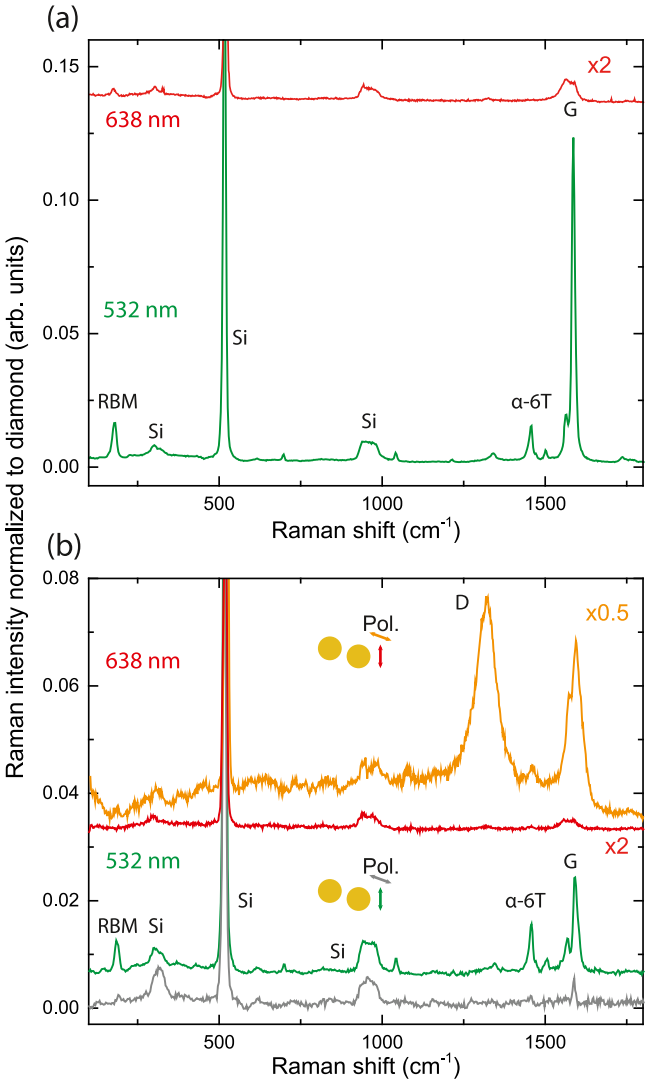

Figure 2. Raman spectra at 532 nm (green) and 638 nm (red) excitation wavelength of (a) reference α-6T@CNT bundle and (b) plasmonically enhanced α-6T@CNT-Au bundle. The spectra are offset for clarity. The prominent Raman modes of the Si substrate, the CNT, and the enclosed α-6T-molecules are labeled. In the plasmonic system in (b), we additionally show different polarizations of the incoming light, as indicated. Green and red indicate the polarization along the CNT axis, while orange and gray indicate the polarization parallel to the dimer axis. The different G mode intensity at 532 nm in panel (a,b) is due to the different nanotube chiralities in the two tube α-6T@CNT bundles as is evident from the different RBM frequencies.

that there is no interaction between the gold surface and the α-6T molecules.[26] It strongly suggests that the encapsulated molecules are not in direct contact with the gold dimer.[26]

3.1. Polarization-Dependent Measurements. We investigated the polarization dependence of the CNT and molecular Raman modes, which reveals the alignment of the molecules inside the CNT and the influence of the plasmonic near field. Figure 4 shows the polarization dependence of both (a) the reference tube bundle and (b) the plasmonically enhanced tube bundle.

The polarization-dependent Raman intensity is described by $I_{pol}(\Theta) = |\boldsymbol{e}_i \cdot R \cdot \boldsymbol{e}_s|^2$ where $\boldsymbol{e}_i$ and $\boldsymbol{e}_s$ are the polarizations of the incoming and scattered light, respectively. The angle Θ is

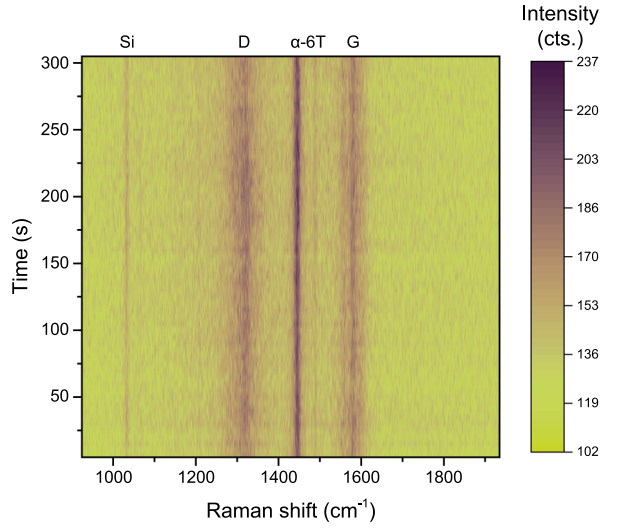

Figure 3. SERS intensity as a function of time. Each line represents a spectrum with 5 s acquisition time. Overall, 60 consecutive Raman spectra were recorded. The CNT and molecular Raman modes are clearly visible and labeled accordingly. The excitation wavelength was 585 nm.

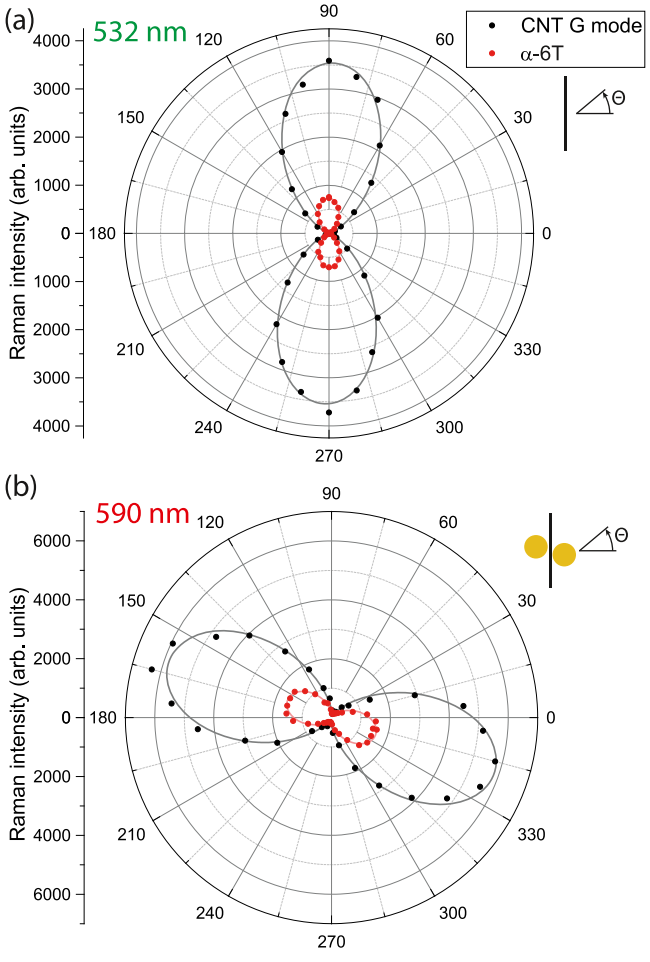

Figure 4. Polarization-dependent Raman measurements of the CNT G-mode (black circles) and the α-6T Raman mode of the (a) reference system at 532 nm excitation wavelength and (b) plasmonic system at 590 nm. The solid lines show the fits according to eq 1.

DOI: 10.1021/acs.jpcc.9b01600
J. Phys. Chem. C 2019, 123, 10578−10585

defined counterclockwise from the horizontal axis within our laboratory frame; see Figure 4a,b. We use a general two dimensional Raman tensor $R = \begin{pmatrix} a & 0 \\ 0 & b \end{pmatrix}$ defined in the plane of the substrate surface.[31] To fit the experimental data shown in Figure 4, we use[3]

$$I_{pol}(\Theta) = a^2 \cos^4(\Theta) + b^2 \sin^4(\Theta) \quad (1)$$

where a and b are the fitting parameters. The fitted parameters are summarized in Table 1.

Table 1. Fitting Parameters of the Polarization-Dependent Measurements According to Eq 1

	reference α-6T@CNT		enhanced α-6T@CNT-Au	
	G	α-6T	G	α-6T
a	2	1	76	40
b	60	27	9	10

For the reference α-6T@CNT in Figure 4a, the intensity maxima for both the tube modes and the molecule modes are found when the polarization is along the nanotube axis. This confirms that the transition dipole moment of the α-6T molecules is aligned along the CNT axis, which is consistent with transmission electron microscopy results.[28] The polarization behavior of CNTs is characterized by a maximum intensity of all Raman modes for a polarization along the tube axis and a minimum intensity for a perpendicular polarization.[31] This is found in the reference α-6T, as well, see Figure 4.

The polarization dependence of the enhanced α-6T@CNT-Au presented in Figure 4b is dominated by the plasmonic near field of the gold dimer.[19] We observe maximum intensity for a polarization along the dimer axis and a small but finite intensity when polarized along the nanotube. The intensity did not drop to zero for a polarization perpendicular to the dimer axis because of the normal Raman scattering process (not plasmonically enhanced) in the α-6T@CNT. We observe a difference of $\Delta\Theta = 68°$ between the angles showing maximum Raman intensity of the plasmonic enhanced and reference α-6T@CNT, which is in excellent agreement with the angle between the reference CNT and the dimer axis measured in the AFM topography (see section 2).

The polarization dependence of the Raman intensity shows the strong influence of the plasmonic near field. It can be used as a fingerprint to confirm the presence of plasmonic enhancement and to distinguish it from other enhancement mechanisms.

3.2. Resonant Raman Measurements. We performed wavelength-dependent Raman measurements to investigate the intrinsic resonance of the encapsulated molecule and the plasmonic enhancement of the molecules. First, we will discuss the intrinsic resonance. We measured a small bundle of α-6T@CNTs; see Figure 1c. We excited the encapsulated molecules with polarization along the tube axis ($\Theta_{mol} = 90°$). By changing the excitation wavelength, we were able to determine the vibronic transition energy of the molecule. In Figure 5a, we show a waterfall plot of Raman spectra at different excitation wavelengths. The molecular mode at 1450 cm^{-1} has a maximum in intensity at 532 nm excitation, whereas it is barely visible at red (655 nm) and blue (462 nm) excitation.

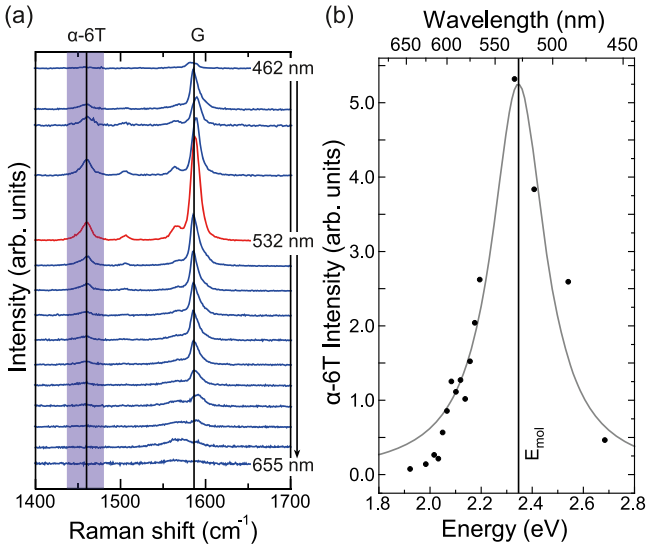

Figure 5. (a) Waterfall plot of Raman spectra at different excitation wavelengths of the reference α-6T@CNT bundle. The excitation wavelength increases from top to bottom. The α-6T Raman mode is indicated by the shaded blue area. The red spectrum marks the molecular resonance energy E_{mol}. (b) Resonant Raman measurements (black dots) of the reference α-6T@CNTs. The area of the molecular Raman mode is plotted over the excitation wavelength. The solid black line shows the resonant Raman fit according to eq 2.

A plot of the integrated area of the molecular Raman mode over the excitation wavelength in Figure 5b shows a clear maximum at 532 nm. We use

$$I_{mol}(E_l) = \left| \frac{M_{mol}}{E_l - E_{mol} - i\gamma_{mol}} \right|^2 \quad (2)$$

to fit the molecular resonance, where M_{mol} is the coupling matrix element, E_l is the laser energy, E_{mol} is the molecular resonance energy, and $\gamma_{mol} = \hbar/\tau_{mol}$ is the inverse vibronic lifetime. Equation 2 corresponds to the resonant Raman intensity derived from the perturbation theory.[3,32] From the fit, we obtain a resonance energy of $E_{mol} = 2.35$ eV (528 nm) and a width of $\gamma_{mol} = 0.13$ eV. The resonance energy is in excellent agreement with the absorption measurements of α-6T@CNTs by Gaufrès et al.[27] Because of the small width of the resonance, we assume only one electronic transition participating in the measured resonance Raman profile.

3.3. Plasmonic Enhancement. We performed the measurements on the plasmonically enhanced α-6T@CNT-Au bundle, see Figure 1b, in a similar way as the reference α-6T@CNT. In contrast to the previous measurements, we excite the plasmonically enhanced molecules with polarization along the dimer axis ($\Theta_{pl} = 160°$). In Figure 6a, we show a waterfall plot with Raman spectra at different excitation wavelengths. The red spectrum marks the wavelength (590 nm) at which we observe the highest enhancement from the plasmonically enhanced α-6T@CNT-Au. Figure 6b shows the integrated area of the α-6T Raman mode plotted over the excitation wavelengths. Compared to the reference α-6T@CNT, we observe a strong shift of the highest Raman enhancement to higher wavelength.

To describe the excitation energy dependence of the plasmon-enhanced Raman signal of the α-6T molecules, we

DOI: 10.1021/acs.jpcc.9b01600
J. Phys. Chem. C 2019, 123, 10578−10585

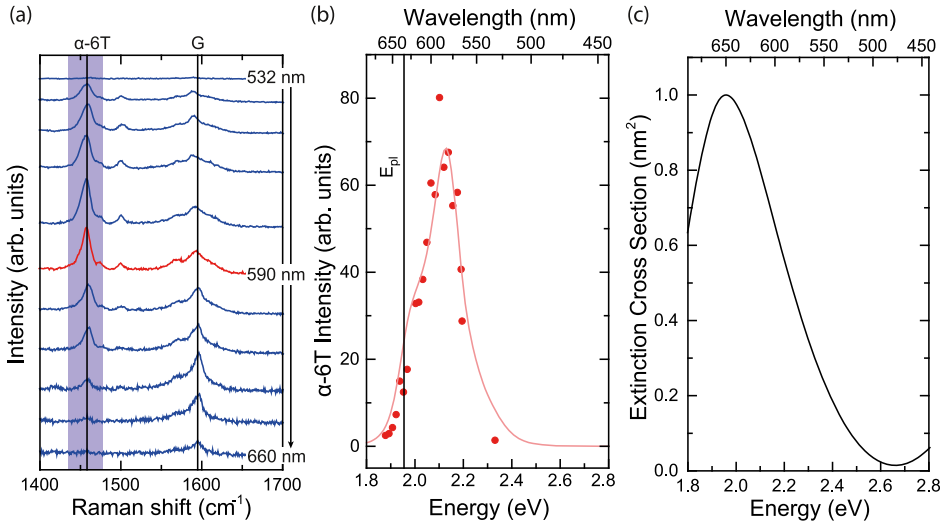

Figure 6. (a) Waterfall plot of Raman spectra of the plasmonic enhanced α-6T@CNT-Au bundle at different excitation wavelengths. The excitation wavelength increases from top to bottom. The α-6T Raman mode is indicated by the shaded blue area. The red spectrum indicates the spectrum with highest enhancement. (b) Resonant Raman measurements of the enhanced CNTs. The integrated area of the molecular Raman mode is plotted over the excitation wavelength. The solid red line shows the fit of the wavelength-dependent Raman measurements (red dots) according to eq 3. (c) FDTD simulation of the extinction cross section of the gold nanodimer as a function of excitation energy.

use higher-order Raman scattering theory that incorporates the plasmonic enhancement in the scattering process[33]

$$I_{\mathrm{SERS}}(E_{\mathrm{l}}) = \left| \frac{M_{\mathrm{pl}} M_{\mathrm{mol}}}{(E_{\mathrm{l}} - \hbar\omega_{\alpha\text{-}6\mathrm{T}} - E_{\mathrm{pl}} - \mathrm{i}\gamma_{\mathrm{pl}})(E_{\mathrm{l}} - E_{\mathrm{mol}} - \mathrm{i}\gamma_{\mathrm{mol}})(E_{\mathrm{l}} - E_{\mathrm{pl}} - \mathrm{i}\gamma_{\mathrm{pl}})} \right|^2 \tag{3}$$

where M_{pl} is the scattering matrix element describing the plasmonic enhancement, E_{pl} is the plasmon energy, γ_{pl} is the inverse plasmonic lifetime, and $\omega_{\alpha\text{-}6\mathrm{T}}$ is the Raman shift of the α-6T mode. By inserting the molecular parameters E_{mol}, γ_{mol}, and M_{mol} as obtained from the reference α-6T@CNT measurement (see section 3.2), we extract the plasmon energy E_{pl} = 1.95 eV (636 nm) and plasmon width γ_{pl} = 0.07 eV. The theory of higher-order Raman scattering predicts different and competing scattering pathways to contribute to the overall enhancement, where the plasmon may take part in the Raman scattering process once or multiple times.[33] In our approach, however, we only include the contribution where the plasmonic near field interacts with the incoming and outgoing light because it yields the strongest enhancement. A full treatment of all possible scattering channels is beyond the scope of this work.

The plasmon resonance is energetically located at E_{pl} = 1.95 eV as expected for gold dimers with similar dimensions.[19,20,34] In Figure 6c, we show a simulation of the extinction cross section of the gold dimer as a function of excitation energy and find the plasmon resonance at 1.95 eV which is in excellent agreement with the experimental data.

The plasmonic near field enhances the Raman scattering process of the CNT and the encapsulated molecules. The maximum enhancement is observed between the vibronic and plasmonic resonance at 2.13 eV because of the overlap of both resonances. It is closer to the plasmon resonance in contrast to the results reported in ref 5. We observe a red shift of maximum enhancement of ΔE = 0.22 eV.

3.4. Enhancement Factor. SERS is used in applications like analytics and biosensing among others.[2,35,36] The performance of different plasmonic systems is compared by their enhancement factors EF. We obtain the enhancement as

$$\mathrm{EF} = \frac{I_{\mathrm{SERS}}}{I_{\mathrm{ref}} \cos^4(\Delta\Theta)} \approx 8 \times 10^3 \tag{4}$$

where I_{SERS} is the integrated Raman intensity of plasmonically enhanced α-6T mode, and I_{ref} is the integrated intensity of the reference α-6T. We obtained an angle of $\Delta\Theta$ = 68° from the polarization measurements (section 3.1) and the AFM measurement (section 2). We calculate the enhancement factor by dividing the Raman intensity of the enhanced α-6T mode for maximum enhancement at 590 nm by the value of the reference fit at the same wavelength (see Figure 5). We have to consider the polarization direction that differed in the SERS and the reference measurement. In case of the reference α-6T@CNT, the polarization was chosen to be along the tube axis (Θ_{mol} = 90°). For the plasmonically enhanced α-6T@CNT-Au, the polarization was along the dimer axis (Θ_{pl} = 160°) activating the plasmonic hotspot in the gap between the two gold discs. From the AFM topography, we estimate the number of nanotubes in the bundle and therefore the number of molecules in this bundle. We calculate the diameter of a single nanotube by the RBM frequency. The relationship is given by

$$\omega_{\mathrm{RBM}} = \frac{c_1}{d} + c_2 \tag{5}$$

with c_1 = 220 cm^{-1} nm and c_2 = 20 cm^{-1}.[37] The plasmonically enhanced bundle shows an RBM at $\omega_{\mathrm{SERS}}^{\mathrm{RBM}}$ = 183 cm^{-1} corresponding to a nanotube diameter of d_{SERS} = 1.30 nm. The reference CNTs exhibit an RBM with frequency $\omega_{\mathrm{ref}}^{\mathrm{RBM}}$ = 190 cm^{-1} corresponding to a diameter of d_{ref} = 1.25 nm. The diameters fit well to the mean diameter of the used CNTs of 1.30 nm (see section 2).

The plasmonically enhanced bundle has a diameter of 9.7 nm corresponding to 55−60 nanotubes. With the length of the molecule l = 2.2 nm, two rows of molecules,[25] and maximum filling of the nanotubes, we find an upper bound of $n_{\mathrm{SERS}} \approx 800$ molecules in the plasmonic hotspot. We assume an effective

DOI: 10.1021/acs.jpcc.9b01600
J. Phys. Chem. C 2019, 123, 10578−10585

size of 15 nm where the plasmonic near field interacts with the α-6T@CNT-Au.[26]

The reference bundle has a height of 6.5 nm corresponding to 25−30 nanotubes in the cross section. For this bundle, we have to consider molecules contributing from the entire laser spot ($fwhm_{las}$ = 450 nm; measured by scanning the laser focus spatially over a nanotube bundle). With these assumptions, we calculate a number of $n_{ref} \approx 9200$ molecules in the reference α-6T@CNT. We estimate an enhancement factor of

$$EF_{mol} = \frac{EF \cdot n_{ref}}{n_{SERS}} \approx 9 \times 10^4 \quad (6)$$

The enhancement factor is in good agreement with measurements on graphene performed on a similar gold dimer system.[20] In conclusion, there are three contributions we have to take into account when comparing the plasmonically enhanced α-6T@CNT-Au with the α-6T@CNT reference: first, we observe different polarizations for the reference and plasmonically enhanced α-6T@CNT. Second, the number of molecules is different for both. It is important to note that we assume maximum filling of the nanotubes in our calculation. If the tubes are not completely filled or some tubes in the bundle are not filled, we expect a higher enhancement factor because the number of molecules in the hotspot influences the enhancement factor more than the number of molecules in the reference bundle. However, a uniform filling over several micrometers was confirmed by hyperspectral Raman images; see ref 25. Third, the estimation of the size of the plasmonic hotspot is crucial to evaluate the enhancement factor. A smaller hotspot size leads to stronger enhancement.

4. CONCLUSIONS

We presented an extensive Raman study of α-6T molecules encapsulated in CNTs. We investigated small bundles of α-6T@CNT with and without plasmonic enhancement. Because we performed the measurements with the same adjacent dielectric and the same measurement conditions, we were able to directly compare the experimental Raman intensities. The α-6T@CNT-Au were deposited in a plasmonic cavity formed by two gold discs by dielectrophoresis. With this method, we were able to deposit a certain amount of molecules into a well-defined plasmonic hotspot. Benefiting from the special geometry of the used setup, we were able to estimate the maximum number of molecules in the plasmonic hotspot. The encapsulation of the α-6T molecules inside of the CNTs protected the molecules. We did not observe any blinking in the Raman spectra of α-6T@CNT-Au, which is an indicator that no chemical enhancement is present. By polarization-dependent Raman measurements, we confirmed the alignment of the molecules along the nanotube axis and observed the strong influence of the plasmonic near field rotating the polarization for strongest Raman intensity to be aligned with the dimer axis. We identified the intrinsic molecular resonance and the plasmonic resonance by wavelength-dependent Raman measurements. We observed a red shift of 0.22 eV of the maximum Raman intensity in the case of the plasmon-enhanced α-6T@CNT-Au, which shows that plasmonic enhancement dominates over the intrinsic molecular enhancement in our case. Encapsulating molecules inside of CNTs opens a promising path to investigate the influence of the plasmonic near field to the protected molecules. In our case of α-6T@CNT-Au placed inside a gold dimer with the used dimensions, the intrinsic molecular and localized surface plasmon resonances are energetically far separated. Using different molecules inside the CNT with an intrinsic resonance overlapping with the plasmonic resonance, it will be possible to separate the individual contributions from the overall enhancement factor by turning the polarization to the dimer or CNT axis.

AUTHOR INFORMATION

Corresponding Author

*E-mail: reich@physik.fu-berlin.de.

ORCID

Sören Wasserroth: 0000-0002-3645-5969
Sebastian Heeg: 0000-0002-6485-3083
Niclas S. Mueller: 0000-0002-8688-1974
Patryk Kusch: 0000-0001-9180-786X
Richard Martel: 0000-0002-9021-4656
Aravind Vijayaraghavan: 0000-0001-8289-2337

Notes

The authors declare no competing financial interest.

ACKNOWLEDGMENTS

This work was supported by the Focus Area NanoScale of Freie Unitversität Berlin. S.H. acknowledges financial support by ETH Zurich Career Seed Grant SEED-16 17-1. S.H. and A.V. acknowledge funding from the Engineering and Physical Sciences Research Council (EPSRC) grant EP/K016946/1. N.S.M. acknowledges Deutsche Telekom Stiftung for financial support. R.M. and N.Y.-W.T. acknowledge support from the NSERC Discovery and the Canada Research Chair programs.

REFERENCES

(1) Fenner, W. R.; Hyatt, H. A.; Kellam, J. M.; Porto, S. P. S. Raman cross section of some simple gases. *J. Opt. Soc. Am.* **1973**, *63*, 73.

(2) Stiles, P. L.; Dieringer, J. A.; Shah, N. C.; Van Duyne, R. P. Surface-Enhanced Raman Spectroscopy. *Annu. Rev. Anal. Chem.* **2008**, *1*, 601−626.

(3) Cardona, M.; Chang, R. K.; Güntherodt, G.; Long, M. B.; Vogt, H.. In *Light Scattering in Solids II*; Cardona, M., Güntherodt, G., Eds.; Springer-Verlag Berlin Heidelberg, 1982.

(4) McFarland, A. D.; Young, M. A.; Dieringer, J. A.; van Duyne, R. P. Wavelength-scanned surface-enhanced Raman excitation spectroscopy. *J. Phys. Chem. B* **2005**, *109*, 11279−11285.

(5) McNay, G.; Eustace, D.; Smith, W. E.; Faulds, K.; Graham, D. Surface-enhanced Raman scattering (SERS) and surface-enhanced resonance Raman scattering (SERRS): a review of applications. *Appl. Spectrosc.* **2011**, *65*, 825−837.

(6) Ding, S.-Y.; Yi, J.; Li, J.-F.; Ren, B.; Wu, D.-Y.; Panneerselvam, R.; Tian, Z.-Q. Nanostructure-based plasmon-enhanced Raman spectroscopy for surface analysis of materials. *Nat. Rev. Mater.* **2016**, *1*, 16036.

(7) Le Ru, E. C.; Etchegoin, P. G. Single-Molecule Surface-Enhanced Raman Spectroscopy. *Annu. Rev. Phys. Chem.* **2012**, *63*, 65−87.

(8) Xu, H.; Aizpurua, J.; Käll, M.; Apell, P. Electromagnetic contributions to single-molecule sensitivity in surface-enhanced Raman scattering. *Phys. Rev. E: Stat., Nonlinear, Soft Matter Phys.* **2000**, *62*, 4318−4324.

(9) Kleinman, S. L.; Ringe, E.; Valley, N.; Wustholz, K. L.; Phillips, E.; Scheidt, K. A.; Schatz, G. C.; Van Duyne, R. P. Single-Molecule Surface-Enhanced Raman Spectroscopy of Crystal Violet Isotopologues: Theory and Experiment. *J. Am. Chem. Soc.* **2011**, *133*, 4115−4122.

DOI: 10.1021/acs.jpcc.9b01600
J. Phys. Chem. C 2019, 123, 10578−10585

(10) Weitz, D. A.; Garoff, S.; Gersten, J. I.; Nitzan, A. The enhancement of Raman scattering, resonance Raman scattering, and fluorescence from molecules adsorbed on a rough silver surface. *J. Chem. Phys.* **1983**, *78*, 5324−5338.
(11) Fleischmann, M.; Hendra, P. J.; McQuillan, A. J. Raman spectra of pyridine adsorbed at a silver electrode. *Chem. Phys. Lett.* **1974**, *26*, 163−166.
(12) Jeanmaire, D.; Van Duyne, R. P. Surface Raman spectroelectrochemistry Part I. Heterocyclic, aromatic, and aliphatic amines adsorbed on the anodized silver electrode. *J. Electroanal. Chem. Interfacial Electrochem.* **1977**, *84*, 1−20.
(13) Haynes, C. L.; McFarland, A. D.; van Duyne, R. P. Surface-Enhanced Raman Spectroscopy. *Anal. Chem.* **2005**, *77*, 338A−346A.
(14) Haran, G.; Chuntonov, L. Artificial Plasmonic Molecules and Their Interaction with Real Molecules. *Chem. Rev.* **2018**, *118*, 5539−5580.
(15) Heeg, S.; Clark, N.; Oikonomou, A.; Vijayaraghavan, A.; Reich, S. Plasmon-enhanced Raman scattering by suspended carbon nanotubes. *Phys. Status Solidi RRL* **2014**, *08*, 785−789.
(16) Park, J.-E.; Jung, Y.; Kim, M.; Nam, J.-M. Quantitative Nanoplasmonics. *ACS Cent. Sci.* **2018**, *4*, 1303−1314.
(17) Murgida, D. H.; Hildebrandt, P. Heterogeneous Electron Transfer of Cytochromecon Coated Silver Electrodes. Electric Field Effects on Structure and Redox Potential. *J. Phys. Chem. B* **2001**, *105*, 1578−1586.
(18) Knight, M. W.; Wu, Y.; Lassiter, J. B.; Nordlander, P.; Halas, N. J. Substrates Matter: Influence of an Adjacent Dielectric on an Individual Plasmonic Nanoparticle. *Nano Lett.* **2009**, *9*, 2188−2192.
(19) Wasserroth, S.; Bisswanger, T.; Mueller, N. S.; Kusch, P.; Heeg, S.; Clark, N.; Schedin, F.; Gorbachev, R.; Reich, S. Graphene as a local probe to investigate near-field properties of plasmonic nanostructures. *Phys. Rev. B* **2018**, *97*, 155417.
(20) Heeg, S.; Fernandez-Garcia, R.; Oikonomou, A.; Schedin, F.; Narula, R.; Maier, S. A.; Vijayaraghavan, A.; Reich, S. Polarized Plasmonic Enhancement by Au Nanostructures Probed through Raman Scattering of Suspended Graphene. *Nano Lett.* **2013**, *13*, 301−308.
(21) Vijayaraghavan, A.; Blatt, S.; Weissenberger, D.; Oron-Carl, M.; Hennrich, F.; Gerthsen, D.; Hahn, H.; Krupke, R. Ultra-large-scale directed assembly of single-walled carbon nanotube devices. *Nano Lett.* **2007**, *7*, 1556−1560.
(22) Heeg, S.; Oikonomou, A.; Fernandez-Garcia, R.; Lehmann, C.; Maier, S. A.; Vijayaraghavan, A.; Reich, S. Plasmon-enhanced Raman scattering by carbon nanotubes optically coupled with near-field cavities. *Nano Lett.* **2014**, *14*, 1762−1768.
(23) Heeg, S.; Clark, N.; Vijayaraghavan, A. Probing hotspots of plasmon-enhanced Raman scattering by nanomanipulation of carbon nanotubes. *Nanotechnology* **2018**, *29*, 465710.
(24) Hirsch, A. Functionalization of Single-Walled Carbon Nanotubes. *Angew. Chem., Int. Ed.* **2002**, *41*, 1853.
(25) Gaufrès, E.; Tang, N. Y.-W.; Favron, A.; Allard, C.; Lapointe, F.; Jourdain, V.; Tahir, S.; Brosseau, C.-N.; Leonelli, R.; Martel, R. Aggregation Control of α-Sexithiophene via Isothermal Encapsulation Inside Single-Walled Carbon Nanotubes. *ACS Nano* **2016**, *10*, 10220−10226.
(26) Mueller, N. S.; Heeg, S.; Kusch, P.; Gaufrès, E.; Tang, N. Y.-W.; Hübner, U.; Martel, R.; Vijayaraghavan, A.; Reich, S. Plasmonic enhancement of SERS measured on molecules in carbon nanotubes. *Faraday Discuss.* **2017**, *205*, 85−103.
(27) Gaufrès, E.; Tang, N. Y.-W.; Lapointe, F.; Cabana, J.; Nadon, M.-A.; Cottenye, N.; Raymond, F.; Szkopek, T.; Martel, R. Giant Raman scattering from J-aggregated dyes inside carbon nanotubes for multispectral imaging. *Nat. Photonics* **2014**, *8*, 72−78.
(28) Loi, M. A.; Gao, J.; Cordella, F.; Blondeau, P.; Menna, E.; Bártová, B.; Hébert, C.; Lazar, S.; Botton, G. A.; Milko, M.; et al. Encapsulation of conjugated oligomers in single-walled carbon nanotubes: towards nanohybrids for photonic devices. *Adv. Mater.* **2010**, *22*, 1635−1639.
(29) Kusch, P.; Mastel, S.; Mueller, N. S.; Morquillas Azpiazu, N.; Heeg, S.; Gorbachev, R.; Schedin, F.; Hübner, U.; Pascual, J. I.; Reich, S.; et al. Dual-Scattering Near-Field Microscope for Correlative Nanoimaging of SERS and Electromagnetic Hotspots. *Nano Lett.* **2017**, *17*, 2667−2673.
(30) Benz, F.; Schmidt, M. K.; Dreismann, A.; Chikkaraddy, R.; Zhang, Y.; Demetriadou, A.; Carnegie, C.; Ohadi, H.; de Nijs, B.; Esteban, R.; et al. Single-molecule optomechanics in "picocavities". *Science* **2016**, *354*, 726−729.
(31) Reich, S.; Thomsen, C.; Maultzsch, J. *Carbon Nanotubes: Basic Concepts and Physical Properties*; John Wiley & Sons, 2008.
(32) Kuzmany, H. The particle in the box model for resonance Raman scattering in polyacetylene. *Pure Appl. Chem.* **1985**, *57*, 235−246.
(33) Mueller, N. S.; Heeg, S.; Reich, S. Surface-enhanced Raman scattering as a higher-order Raman process. *Phys. Rev. A* **2016**, *94*, 023813.
(34) Le, K. Q.; Alù, A.; Bai, J. Multiple Fano interferences in a plasmonic metamolecule consisting of asymmetric metallic nanodimers. *J. Appl. Phys.* **2015**, *117*, 023118.
(35) Petryayeva, E.; Krull, U. J. Localized surface plasmon resonance: Nanostructures, bioassays and biosensing-A review. *Anal. Chim. Acta* **2011**, *706*, 8−24.
(36) Li, Q.-l.; Li, B.-w.; Wang, Y.-q. Surface-enhanced Raman scattering microfluidic sensor. *RSC Adv.* **2013**, *3*, 13015−13026.
(37) Maultzsch, J.; Telg, H.; Reich, S.; Thomsen, C. Radial breathing mode of single-walled carbon nanotubes: Optical transition energies and chiral-index assignment. *Phys. Rev. B: Condens. Matter Mater. Phys.* **2005**, *72*, 4077.

DOI: 10.1021/acs.jpcc.9b01600
J. Phys. Chem. C 2019, 123, 10578−10585